PCCP

Accepted Manuscript

ROYAL SOCIETY OF CHEMISTRY

www.rsc.org/pccp

Cite this: DOI: 10.1039/c0xx00000x

www.rsc.org/xxxxxx

ARTICLE TYPE

Spectroscopy and Dynamics of the HOCO Radical: Insights into the OH + CO → H + CO_2 Reaction

Christopher J. Johnson,[a] Rico Otto [b] and Robert E. Continetti*[b]

Received (in XXX, XXX) 9th June 2014, Accepted Xth XXXXXXXXX 20XX

DOI: 10.1039/b000000x

After more than forty years of scrutiny, crucial new details regarding the elementary reaction OH + CO → H + CO_2 are still emerging from experimental and theoretical studies of the HOCO radical intermediate. In this perspective, previous studies of this elementary reaction and the structure and energetics of the HOCO radical will be briefly reviewed. Particular attention will be paid to the experimental techniques used in our laboratory to prepare excited HOCO radicals by both photodetachment and dissociative photodetachment of $HOCO^-$. These experiments directly probe the dynamics occurring on the ground and excited states of the HOCO radical, and are sensitive to both direct and tunneling-induced dissociation. Photoelectron-photofragment coincidence experiments on $HOCO^-$ in particular have been used to study tunneling from the HOCO well to form H + CO_2 products. In addition, new experimental insights into the OH + CO entrance channel for the reaction will be presented. These studies have provided a number of constraints on the potential energy surface for this system from an energetic and dynamical perspective, and have helped spur a renewed effort to characterize the global potential energy surface and reaction dynamics of this fundamental chemical reaction. Outstanding questions and new directions for future work on the HOCO radical will be discussed.

Introduction

The hydroxycarbonyl (HOCO) free radical is an important intermediate in the bimolecular reaction between the hydroxyl radical and carbon monoxide, OH + CO → H + CO_2. Increasingly, this system is also serving as a benchmark reaction for understanding the dynamics of complex-forming polyatomic reactions with multiple product channels.[1] Over the last four decades, this reaction has been the focus of intense interest as a result of its importance in determining the CO/CO_2 balance in combustion and atmospheric chemistry, and the role it plays in the release of heat during hydrocarbon combustion.[2-4] HOCO is also expected to play an important role in the tropospheric chemistry on Earth as well as CO_2-dominated planetary atmospheres such as that on Mars.[5] Given this significance, a broad range of experimental and theoretical studies have been carried out to understand the structure and energetics of HOCO and the reaction kinetics and dynamics of the OH + CO → H + CO_2 reaction. A particular focus of this perspective will be the recent experimental work from our laboratory using photodetachment and dissociative photodetachment (DPD) of $HOCO^-$ to characterize the HOCO radical and the potential energy surface governing the OH + CO → H + CO_2 reaction in the context of recent theoretical advances. Progress made in experimentally determining the barrier to tunneling from *cis*-HOCO to H + CO_2,[6] new spectroscopic information on *cis*- and *trans*-HOCO and DOCO including vibrational frequencies and electron affinities,[7] as well as the implications of the experiments on understanding the competition between dissociation of HOCO to OH + CO and H + CO_2 will be reviewed.

Kinetics, Dynamics and Spectroscopy

The oxidation of CO by the OH radical is one of the terminal steps in combustion, providing an impetus for the numerous studies of the kinetics and dynamics of this reaction. Smith and Zellner first proposed that the inverse pressure dependence of the OH + CO reaction rate was consistent with a radical intermediate, HOCO.[8] This led to a number of efforts to study the pressure and temperature dependence of the rate of the OH + CO reaction, providing evidence for a deep HOCO well and a barrier above the OH + CO entrance channel leading to the formation of H + CO_2.[9-18] Experimental studies of the reaction dynamics of both OH + CO and H + CO_2 collisions have also been pursued. Inelastic and reactive collisions of OH + CO were studied by crossed-molecular beam scattering[19-21] and transient FTIR spectroscopy.[22] The reverse reaction of H + CO_2 has been studied in van der Waals clusters, including time-resolved measurements,[23-25] as well as true bimolecular collisions.[26, 27] These studies provided information on the partitioning of energy in the products as well as integral and differential cross sections.

Once the HOCO radical was identified as an intermediate, significant effort was directed towards the spectroscopic identification and characterization of the molecular structure. Both *cis*- and *trans*- isomers of HOCO and the deuterated form DOCO were first observed in cryogenic matrices, and matrix values for all the vibrational frequencies have been reported.[28-30] In the early 1990's the H-O and terminal CO stretch vibrations were observed in the infrared (IR) for gas-phase *trans*-HOCO and DOCO[31-34] and rotational constants were determined from microwave and far-IR spectra.[35-37] High-resolution rotational spectra for both *cis*- and *trans*-HOCO and DOCO have been reported by Endo and co-workers, confirming the molecular structure and indicating that in a pulsed discharge on CO/Ar/H_2O nearly equal populations of the *cis*- and *trans*- isomers were formed.[38] Finally, Nesbitt and co-workers have recently reported sub-Doppler measurements of the OH stretching mode in *trans*-HOCO.[39] However, there remained significant gaps in experimental observations of the vibrational levels of isolated HOCO/DOCO. A number of high-level quantum chemistry studies of *cis*- and *trans*-HOCO radicals have recently been reported, seeking to provide spectroscopic quality predictions that will be useful in future experimental efforts. [7,40-43,44]

The HOCO Potential Energy Surface and Dynamics

Theoretical efforts on this system have concentrated on calculation of an accurate potential energy surface (PES) for the ground electronic state (X^2A') of the HOCO complex that governs the OH + CO → H + CO_2 reaction. McLean and Ellinger reported *ab initio* predictions for the two planar isomers, *trans*- and *cis*-HOCO.[45, 46] Several groups have studied the HOCO PES at different levels of theory, beginning with the transition states and local minima along the OH + CO reaction path.[15, 47] A global PES for the H + CO_2 reaction was presented by Schatz *et al.*, using singly and doubly excited configuration interaction calculations and a many-body expansion fit.[48] This surface has been improved several times over the following years.[49-52] A number of other attempts to develop partial or full-dimensional HOCO PESs have been made using a variety of different methods.[53-56] Recently new high-level calculations of the stationary points on the HOCO potential energy surface have been published using the HEAT method[57, 58] and CCSD(T)-F12 level of theory.[59] Bowman, Guo and co-workers have fit a new global potential energy surface to some 35,000 points,[59, 60] while Stanton and co-workers used the stationary points to calculate reaction rate coefficients using semiclassical transition state theory.[57, 58] Finally, a new global potential energy surface based on calculations at the UCCSD(T)-F12/AVTZ level of theory has been reported by Zhang and co-workers using the neural network approach.[61]

Table 1 Theoretical prediction of relative energies for HOCO system (eV)†

	CCF[a]	DFF[c]	YMS[c]	VHK[d]	SLHW[e]	WNSB[f]	DBG[g]
OH + CO	0.00	0.00	0.00 (-0.06)	0.00	0.00	0.00 (-0.07)	0.00
trans-HO···CO (tTS1)			0.02 (-0.05)	0.04	-0.03	0.04 (-0.04)	0.04
cis-HO···CO(cTS1)			0.18 (0.11)	0.17	0.14	*	0.19
OH···CO (hb1)			-0.04 (-0.12)	-0.01	-0.04	-	-0.04
OH···OC (hb2)			-0.01 (-0.08)	0.01	-0.01	-	-0.02
trans-HOCO (min)	-1.19	-1.10	-1.10 (-1.19)	-1.06	-1.00	-1.08 (-1.17)	-1.08
cis-trans-HOCO (τ-TS)			-0.74 (-0.83)	-0.73	-0.64	-0.72 (-0.80)	-0.72
cis-HOCO (min)	-1.11		-1.03 (-1.11)	-0.92	-0.92	-1.01 (-1.10)	-1.01
cis-H···OCO (cTS2)			0.04 (0.02)	0.05	0.11	0.08 (0.06)	0.08
trans-HOCO (cTS4)			0.37 (0.33)	0.40	0.49	0.41 (0.37)	0.41
C_{2v}-HCO_2 (min)			-0.43 (-0.51)	-0.46	-0.47	-	-0.48
C_{2v}-HCO_2 (TS)			-0.45 (-0.47)	-0.44	-0.47	-	-0.40
H···OCO (vdw)			-1.07 (-1.07)	-1.07		-	
H + CO_2			-1.07 (-1.07)	-1.07	-1.05	-1.07 (-1.07)	-1.08
trans-$HOCO^-$	-2.49	-2.46				-2.45 (-2.54)	
cis-$HOCO^-$	-2.54	-2.52				-2.51 (-2.60)	
AEA *trans*-HOCO	1.30	1.36				1.37 (1.37)	
AEA *cis*-HOCO	1.43					1.50 (1.50)	

†All energies have been corrected by ZPEs, referenced to the OH + CO entrance channel, values for DOCO are in parenthesis; [a] CCF: Clements, Continetti, and Francisco,[62] the reference for the OH + CO asymptote was determined by the calculated energetics of OH^- + CO in ref. 62 and the EA(OH) = 1.8277 eV;[63] [b] DFF: Dixon, Feller, and Francisco, ref. 64; Note that $\Delta_f H^0$ (OH) = 8.85 ± 0.07 kcal/mol[65] and a calculated $\Delta_f H^0$ (CO) = -27.0 kcal/mol[66] was used to obtain the OH + CO asymptote in DFF; [c] YMS: Yu, Muckerman, and Sears, ref. 51, in parentheses, energetics of species involved in the OD + CO → D + CO_2 reaction; [d] VHK: Valero, van Hemert, and Kroes, ref. 55; [e] SLHW: Song, Li, Hou, and Wang, ref. 56; [f] WNSB: Nguyen, Xue, Weston Barker and Stanton, ref. 57 and Weston, Nguyen, Stanton and Barker, ref. 58. [g] DBG: Li, Xie, Ma, Wang, Dawes, Xie, Bowman and Guo, ref. 60.

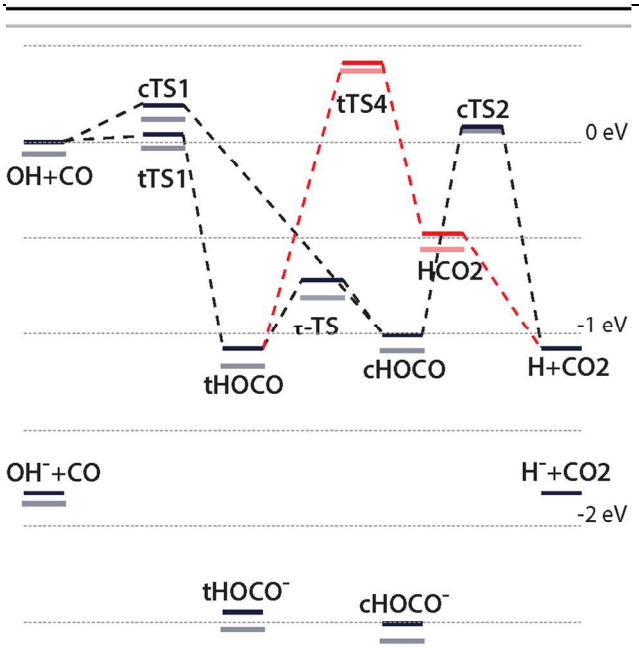

Fig. 1 Ab initio energetics for HOCO/HOCO$^-$ (black lines) and DOCO/DOCO$^-$ (gray lines). Dashed lines indicate the connectivity of the various stationary points. The bold and gray lines at the top of the figure indicate the maximum energy accessible using 3.20 eV photons in the DPD experiments, assuming the initial species is *cis*-HOCO$^-$/*cis*-DOCO$^-$. The energy scale is referenced so that the OH + CO asymptote is at 0.0 eV. Stationary points for the HCO_2/DCO_2 isomer are colored dark/light red.

The zero-point energy corrected energetics of the HOCO system obtained from several recent high-level calculations are summarized in Table 1, using the OH + CO entrance channel as the reference. This comparison of the most recent high level *ab initio* calculations shows that a consensus on the energetics of the stationary points and asymptotic product energies has emerged.[57, 58,59, 60]

As a four-atom system, the reaction coordinate diagrams for HOCO begin to show the rich chemistry expected for polyatomic molecules. Calculations indicate that *trans*-HOCO is more stable than *cis*-HOCO by 0.07 eV, with an out-of-plane torsional isomerization barrier (τ-TS in Fig. 1) 0.36 eV higher than *trans*-HOCO.[51, 52, 55, 56] Following the relaxed minimum energy path along the reaction coordinate for OH + CO, *trans*-HOCO is initially formed via a transition state *trans*-HO···CO TS1 (tTS1) 0.04 eV above the OH + CO asymptote (see Table 1),[51, 55, 56] followed by isomerization to the *cis*-HOCO conformer.

Two hydrogen bonded complexes OH···CO (hb1) and OH···OC (hb2) (not shown in Fig. 1) are predicted in the entrance channel OH + CO. It has been proposed that these play important roles in the abnormal temperature and pressure dependence of the reaction rate coefficients.[67, 68] Lester and co-workers reported spectroscopic evidence for the OH···CO (hb1) complex.[68-70] An alternative entrance channel pathway involves surmounting the higher barrier cTS1 for the direct formation of *cis*-HOCO, 0.19 eV above the OH + CO entrance channel as calculated in refs. [59, 60]. However, this has been found to be a second order transition state with a reaction coordinate that merges with the path leading to *trans*-HOCO.[71,57,60] The saddle point (*c*TS2) separating the *cis*-HOCO complex and the exit channel H + CO_2 lies above the OH + CO entrance channel by 0.08 eV and is characterized by a high imaginary frequency (2053*i* cm^{-1}),[51] consistent with kinetics data indicating that H + CO_2 products are formed by tunneling through the barrier.[12, 15, 53] An alternative reaction path involves *trans*-HOCO converting to the C_{2v} symmetry H·CO_2 conformer over a high barrier (tTS4), forming the formyloxyl radical HCO_2 prior to rapid dissociation into H + CO_2.[49-51, 56] The topology of this reactive surface is summarized in Fig. 1, with the numeric values based on the stationary points calculated by Stanton and co-workers[57, 58] and Bowman, Guo and co-workers.[59, 60] All stationary points have A′ symmetry with the exception of τ-TS, the *cis-trans* isomerization transition state, with A″ symmetry, and the formyloxyl stationary points C_{2v}-HCO_2 (min) and C_{2v}-HCO_2 (TS) indicated in Table 1, with nominal C_{2v} symmetry.

With the global PESs now available for the HOCO system, there have been a number of theoretical studies of the dynamics of the OH + CO reaction. These have included quasiclassical trajectory calculations,[49, 50, 52, 67, 72, 73] followed in recent years by full quantum dynamics calculations.[56, 72, 74-80] Even the newest PESs have been used to calculate rate constants, investigate tunneling phenomena,[57, 58] and calculate differential cross sections[56] and excitation functions.[61]

Dissociative Photodetachment and Charge Exchange

Experiments directly probing the complex dynamics of the HOCO radical itself have been few in number. As noted earlier, there have been a number of spectroscopic studies characterizing the HOCO radical at low levels of internal excitation, along with crossed beam and kinetics studies sensitive to barriers on the OH + CO → H + CO_2 PES. Direct measurements of the depth of the HOCO well and the heat of formation of HOCO have been particularly elusive. Following early attempts to obtain a heat of formation of the HOCO radical from mass spectrometric measurements of appearance potentials,[81, 82] Ruscic *et al.* obtained $\Delta_f H^0_{0K} \geq -45.8 \pm 0.7$ kcal/mol by photoionization of the HOCO radical,[83, 84] consistent with a HOCO well stable by < 1.20 eV relative to the OH + CO asymptote. New approaches to experimentally characterize the dynamics of the HOCO radical over a wide range of internal energies were needed.

One approach to this problem is to prepare energized radicals by neutralization of ionic precursors, and in the case of HOCO, both cation ($HOCO^+$) and anion ($HOCO^-$) precursors are available. The existence of stable, bound ionic precursors is essential to these approaches. The $HOCO^+$ cation provides an excellent platform for probing the neutral HOCO PES by charge exchange, since it was observed as a stable product of the reaction of H_3^+ + CO_2 more than 40 years ago.[85] Even at the highest levels of theory, it has been shown that the trans-$HOCO^+$ cation is the only stable form, with no minimum for cis-$HOCO^+$ or H-CO_2^+.[86]

In the case of the $HOCO^-$ anion, the first evidence for this species in the gas phase was reported in studies of the reaction of H_3O^- + CO using a flowing afterglow that revealed a negative ion product at m/e = 45 that was determined to not be the more stable formate anion, HCO_2^-.[87] The formate anion, HCO_2^-, is well-known and has been observed in condensed phases, including by matrix isolation spectroscopy[30] and recently in the gas-phase by IR-absorption/vibrational predissociation spectroscopy.[73] HCO_2^-

is considerably more stable than $HOCO^-$: the corresponding HCO_2 (formyloxyl) radical has an electron affinity (EA) of 3.50 eV[88] compared to ≤ 1.5 eV for HOCO. In the case of the formyloxyl radical, the H atom is bound to the central carbon, and there are several low-lying electronic states that have been studied by photodetachment.[88-91] In our laboratory, however, it was determined that the lower stability $HOCO^-$ anion could be synthesized by first producing O^- in a discharge or by electron impact on N_2O, reacting that with CH_4 to form OH^- followed by a three-body recombination with CO in a supersonic expansion ion source.[62]

Both ion neutralization approaches have been pursued in our laboratory to prepare HOCO: charge-exchange neutralization of $HOCO^+$ with caesium was used to directly probe highly excited states of the HOCO radical and the dissociative product channels H + CO_2 and OH + CO.[92] To probe the ground state HOCO radical at excitation energies up to and above the opening of the OH + CO channel, however, photodetachment of $HOCO^-$ is an ideal approach.[62, 93] At photon energies > 2.5 eV photodetachment leads to production of stable HOCO along with DPD to both the OH + CO and H + CO_2 product channels:

$$HOCO^- + h\nu \rightarrow HOCO + e^- \quad (1)$$
$$HOCO^- + h\nu \rightarrow OH + CO + e^- \quad (2)$$
$$HOCO^- + h\nu \rightarrow H + CO_2 + e^- \quad (3).$$

If internally cold precursor anions can be generated, the photon energy along with measurement of the photoelectron energy in a coincidence experiment fixes the total energy in the nascent neutral radical. High-resolution photoelectron spectra can provide structural information on the radical at low levels of internal excitation and photoelectron-photofragment coincidence measurements of DPD processes yield direct information on the dissociation processes, both direct and via tunneling, to the OH + CO and H + CO_2 product channels. The insights gained from photodetachment and DPD experiments like these are the primary focus of this manuscript, following a review of the experimental techniques.

Experimental Techniques

Neutralization studies using fast-ion-beam instruments with multiparticle coincidence detection systems enable kinematically complete studies of both charge exchange[94] and DPD processes.[95,96,97] Both of these techniques allow the production of intermediates in neutral reactions that are difficult to prepare by other means. The subsequent dynamics on the neutral PES can lead to dissociation to the entrance or exit asymptotes, or both, of the overall reaction, depending on the Franck-Condon region accessed in the neutralization process. The two approaches generally probe complementary regions on the neutral PES owing to the difference in Franck-Condon regions for photodetachment of anionic precursors or charge exchange of cation precursors. In this way, the intermediate or transition state can be probed, and the ensuing dynamics can be measured to provide direct insight into the overall dynamics on the PES governing the reaction. In the following section, we will focus on advances in the experimental techniques used to study DPD as applied to examination of the spectroscopy and dynamics of HOCO.

Photoelectron-Photofragment Coincidence Spectroscopy

Photoelectron-photofragment-coincidence (PPC) spectroscopy allows the dissociation dynamics of reaction intermediates to be measured as a function of internal energy in the intermediate. Photodetachment of an anionic precursor yields an excited neutral species, with the level of excitation determined by the measured energy of the photoelectron, as in a standard photoelectron spectroscopy experiment. If the resulting neutral is unstable dissociation into two or more fragments can occur, otherwise a stable radical will be detected. Coincidence detection on an event-by-event basis of all the products (electron + stable radical or electron + fragments) with time- and position-sensitive detectors provides a complete kinematic description of the process.

This experiment was carried out using a fast-ion-beam PPC spectrometer.[96, 97] As noted above, $HOCO^-$ was generated in a pulsed supersonic expansion of CH_4, CO, N_2O, and Ar, with a pulsed coaxial discharge and crossed keV electron beam acting on the expansion near the orifice. The expansion was skimmed

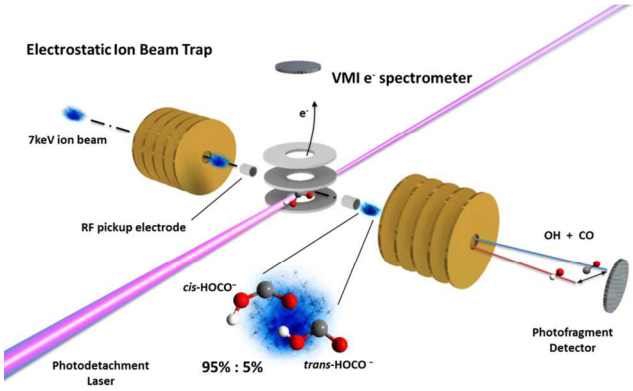

Fig. 2 Schematic of the fast-ion beam PPC spectrometer using a cryogenically cooled electrostatic ion beam trap. Injected ions are bunched and synchronized with the photodetachment laser such that photodetachment occurs when the ions are traveling towards the photofragment detector, allowing the photoelectron and photofragments to be detected in coincidence.

coaxially, electrostatically accelerated to 7 keV, and re-referenced to ground in a fast potential switch. The resulting nearly monoenergetic beam ($\Delta E/E \leq 10^{-3}$) was mass selected by time-of-flight and the mass of interest was intersected by the output of a ~1 kHz picosecond pulsed Ti:Sapphire (Ti:Sa) regenerative amplifier (Clark-MXR CPA-2000) or in some cases a picosecond optical parametric amplifier (Light Conversion TOPAS 4/400) pumped by the second harmonic of the CPA-2000. Photodetached electrons were extracted perpendicularly to the laser-ion plane into a velocity-mapping time- and position sensitive electron detector, which allowed determination of the centre-of-mass (CM) electron kinetic energy (eKE). The CM of the recoiling neutral fragments continued along the ion beam direction, reaching a time- and position-sensitive multiparticle detector where the neutral products were detected with high-efficiency following impact on a microchannel plate. Given the parent ion beam momentum, the distribution of fragment times-of-arrival and positions allowed determination of the three-

dimensional neutral particle momenta, yielding the CM kinetic energy release (KER) with a resolution ΔKER/KER ~ 10% and the product mass ratio with a similar resolution, easily enough to discriminate H + CO_2 from OH + CO.

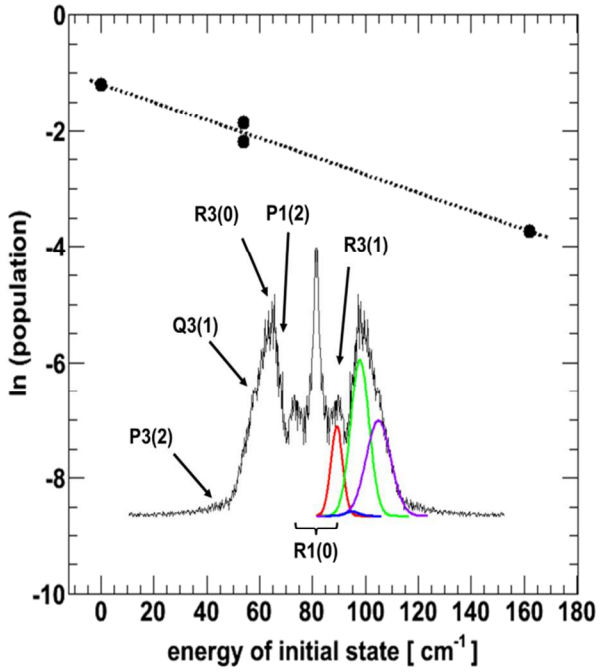

Fig. 3 Thermometry of OH^- anions in the EIBT. The assigned spectrum is the recorded radial eKE spectrum following ref. 98. The x-axis corresponds to the energies of the OH^- (J=0, 1 and 2) states, with the populations deduced from the R3(0), R3(1) and Q3(1), and P1(2) transitions, respectively.

In the most recent experiments, this technique has been enhanced by the addition of a cryogenic electrostatic ion beam trap (EIBT), shown schematically in Fig. 2 and described in detail elsewhere.[97] Briefly, the EIBT is a linear resonator for high-energy ions that is composed of two focusing electrostatic mirrors. Ions are injected through one mirror while it is grounded, then this mirror is rapidly switched to high voltage prior to the first reflection of the ion packet. The ion bunch can be maintained with a small (~1V amplitude) radiofrequency (RF) waveform applied to an intracavity metallic cylinder. A typical ion oscillation frequency for $HOCO^-$ at 7 keV is ~154 kHz, and using an RF signal phase-locked to the oscillator of the Ti:Sa laser, the ion packet can be synchronized with the ~1 kHz laser pulses and intersected when it is moving in the direction of the multiparticle detector used to measure the neutral products. The critical feature of this type of ion trap is a large central field-free region between the mirrors, which serves as an ideal location for laser-ion interaction and electron detection. By performing this experiment inside the trap, it is possible to decouple the ion source rate (~1-10 Hz) from the laser repetition rate. This allows the use of much more intense pulsed supersonic expansions, yielding colder anions initially, and these ions can continue to cool while stored in a cryogenic environment for up to 10 seconds.

It is not possible to measure the temperature of the $HOCO^-$ anions directly. However, using rotationally resolved photoelectron spectroscopy, the temperature of OH^- anions produced in this ion source and measured in the EIBT was determined. The OH^- anion provides an excellent test system, as it has a relatively simple and well known spectrum with widely spaced rotational levels in the vibrational ground state.[98] The rotational structure has been previously observed in near threshold photodetachment experiments given the relatively large rotational spacing (B_0 = 18.7352cm^{-1}).[99] Since individual rotational branches can be resolved in the photodetachment spectrum, this species provides an excellent tool to determine internal (rotational) energies.[100] In these experiments OH^- anions were trapped in the EIBT and irradiated with tunable laser light close to the photodetachment threshold (~680 nm). A typical photoelectron spectrum measured at 674.4 nm is shown as the inset in Fig. 3. The different peaks in the spectrum are assigned to P, Q and R branches, respectively, and have been fit assuming a Gaussian peak shape. The employed wavelength corresponds to the R1(0) threshold (for notation see ref. [98]), as observed at the lowest eKEs. Other transitions with thresholds at lower photon energies are also observed in the spectrum. Since the intensities of the different rotational branches are proportional to the (thermal) population in the anion rotational levels, the spectra allow for a determination of the rotational temperature of the trapped ion ensemble. Taking into account the Hönl-London factors for the rotational transitions[99] the natural logarithm of the populations for OH^- (J=0, 1 and 2) are plotted as a function of rotational energy in Fig. 3. The slope of the linear fit indicates a rotational temperature of 64 ± 5 K. These experiments represent the first rotationally resolved measurements in this fast ion beam experiment and provide an estimate of the rotational temperatures expected for $HOCO^-$.

Photoelectron Spectroscopy of the HOCO Radical

Prior to the experiments described here, there was no previous spectroscopic characterization of the $HOCO^-$ anion used as a precursor to the formation of the HOCO radical. Here, we will discuss insights into $HOCO^-$ and the bound HOCO intermediate ascertained from photoelectron spectroscopy experiments at photon energies above the adiabatic electron affinity (AEA) but below the dissociation thresholds to OH + CO or H + CO_2. The first photoelectron spectra for $HOCO^-$ were measured by Clements *et al.*,[62] but for the spectroscopic electron affinities and vibrational spectra discussed here, we will focus on the more recent high-resolution measurements on cold anions reported by Johnson *et al.* in 2011.[7]

Electron Affinities

Photoelectron spectra near threshold at 775 nm (1.60 eV) allow accurate determination of the AEAs of *cis*- and *trans*-HOCO (1.51 eV and 1.38 eV, respectively) and DOCO (1.51 eV and 1.37 eV, respectively), with an error of ±0.01 eV. Calculations performed using the high-accuracy extrapolated ab initio thermochemistry protocol HEAT345-(Q) reproduce these values to within experimental error.[7] These AEAs represent a significant revision from earlier CCSD(T)//6-311++G(3df,3pd) calculations of 1.43 eV and 1.30 eV for *cis*- and *trans*-HOCO,

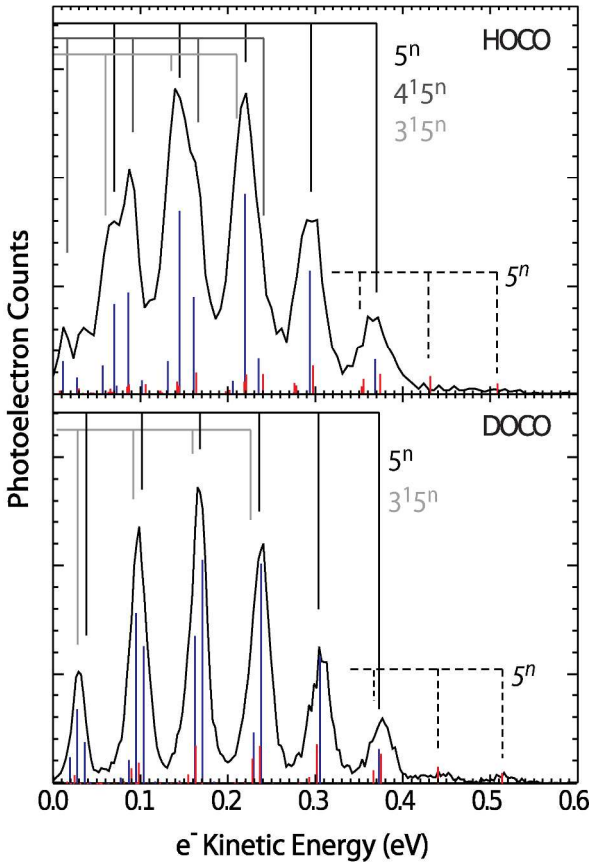

Fig. 4 Photoelectron spectra of $HOCO^-$ (top) and $DOCO^-$ (bottom) recorded at 660 nm (1.88 eV). Also shown are stick spectra from Franck-Condon calculations for *cis* (red) and *trans* (blue) isomers. Dominant sequences are highlighted by the combs above each spectrum.

respectively [ref. 62 see Table 1 for additional reported numbers].

Vibrational Spectroscopy

High-resolution vibrationally resolved photoelectron spectra were measured for both *cis*- and *trans*-$HOCO^-$ and $DOCO^-$ following incorporation of the cryogenically cooled EIBT on the fast beam photoelectron spectrometer. Spectra for $HOCO^-$ and $DOCO^-$ at 660 nm (1.88 eV) are shown in Fig. 4, along with predicted Franck-Condon stick spectra for each isomer of each isotopolog.[7] These spectra are dominated by progressions in the ν_5 (OCO bending) mode, and the DOCO spectrum appears drastically simplified compared to HOCO. These trends are well reproduced by the Franck-Condon simulations based on the *ab initio* HEAT345-(Q) calculations reported in reference 7. Using the Franck-Condon intensities as a guide, it was possible to fit these spectra to determine the gas phase frequencies of the ν_3 (HOC bending), ν_4 (central CO stretching), and ν_5 vibrations of *cis*- and *trans*-HOCO, and the ν_3 and ν_5 vibrations of *cis*- and *trans*-DOCO. These modes had previously only been observed in matrix isolation experiments.[28-30] The ν_1 (OH stretching)[32, 33] and ν_2 (CO stretching)[31] modes of both isomers were previously measured by absorption techniques in the gas phase and were not found to be excited in photodetachment. Both the anion and neutral geometries are planar, precluding observation of the ν_6 torsional bend. These results have recently been confirmed by full-dimensional time-dependent quantum dynamics calculations by Guo and co-workers.[101]

These results provide a second measure of anion internal temperature in addition to the studies of OH^- discussed above: the relative populations of the two isomers. Given the measured AEAs, the populations allow extraction of an ion internal temperature using a two-level Boltzmann model. Fitting the simulated Franck-Condon spectra for each isomer to the measured spectra allows estimation of the population of *cis* and *trans* isomers in the beam. The simulated spectra were corrected for Wigner threshold effects and convolved with an eKE-dependent Gaussian function representing the observed experimental resolution. This process was carried out at two different photodetachment wavelengths, 775 and 660 nm, yielding internally-consistent estimates of 96% cis-HOCO and 94% cis-DOCO and an 'isomeric' electronic temperature of 220K.[7]

Photoelectron Angular Distributions and Resonant Two-Photon Detachment

Photoelectron angular distributions were measured for $HOCO^-$ at a number of wavelengths. Far above the photodetachment threshold the angular distribution peaks strongly along the electric vector of the laser, consistent with *p*-wave photodetachment. Lu *et al.* reported an integrated anisotropy parameter $\beta_e > 1$ for DPD of $HOCO^-$ to both OH + CO + e^- and H + CO_2 + e^- at a photon energy of 3.2 eV.[102] In the vibrationally resolved measurements reported by Johnson *et al.* closer to

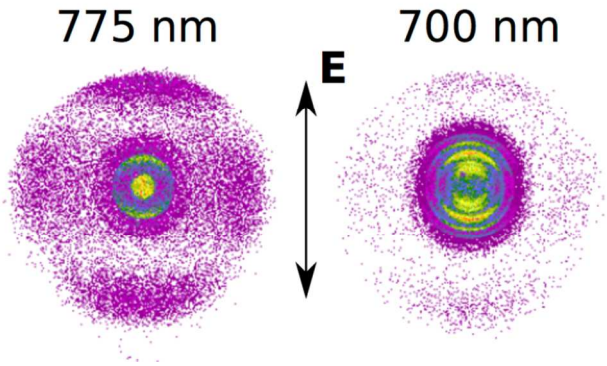

Fig. 5 Raw photoelectron images for $HOCO^-$ photodetachment at 1.60 eV (left) and 1.77 eV (right). The four-fold angular distribution at large radii arising from two-photon detachment is present in both images. These images are clipped at the top due to the increased magnification used to probe the vibrational structure of the inner one-photon signal and the velocity of the incident ion beam.

threshold, for photodetachment to stable HOCO radicals, it was observed that $\beta_e > 1$ for both *cis*- and *trans*- radicals for eKE > 0.15 eV, consistent with *p*-wave photodetachment. Below 0.15 eV, the distribution was observed to be isotropic, consistent with *s*-wave photodetachment. Significant modulation in β_e as a function of final vibrational state was also observed.[7] These results have not been thoroughly interpreted, however, they are consistent with vibrational effects observed in the photoelectron

angular distributions for O_2^- arising from radial dependencies on photodetachment cross-sections.[103]

The most striking phenomenon observed in the photoelectron angular distributions for $HOCO^-$, however, is the distinct four-fold photoelectron angular distribution observed in two-photon photodetachment near threshold. Two-photon photodetachment was first observed in earlier photodetachment experiments at 772 nm using internally hot anions.[104] This signal was attributed to alignment of the anionic precursors by the first photon followed by photodetachment of the excited anions by a second photon. This process was unexpected because the photon energy is above the photodetachment threshold and the photon flux is well below the high-field regime required for more exotic multiphoton interactions to take place.[105] It was proposed that the first photon was absorbed by an excited anionic state or an electron-molecule resonance lying near the detachment threshold. Given that there are no known low-lying electronic excited states of $HOCO^-$, the possibility exists for shape resonances, dipole-bound states, and Feshbach resonances in this energy range. A theoretical study by Miyabe *et al.* found no shape resonances at these energies, and instead suggested that the resonance is a Feshbach resonance supported by dipole-bound anion states.[106] Their calculations predicted *cis*- and *trans*-HOCO to have large dipole moments; 1.86 and 2.84 Debye, respectively, at the MP2 level of theory using Dunning's triple-ζ Gaussian-orbital basis set supplemented with diffuse primitive Gaussian functions.[106] In more recent experiments, the characteristic two-photon signal was also observed at 775 nm using the EIBT, and furthermore observed over a range of photon energies from 1.60 to 1.77 eV. This confirms that the resonance(s) responsible for this effect must be broad, consistent with a dense manifold of dipole-bound states. To illustrate these phenomena, images recorded at 1.60 and 1.77 eV are shown in Fig. 5. This data was recorded under conditions that provided higher resolution spectra of the low-eKE one-photon signal at the centre of the image, so the photoelectrons observed at high eKE from two-photon photodetachment are truncated at the edge of the detector, but the images clearly show that this phenomenon persists at both wavelengths.

Ground State Dissociation Dynamics

Overview of the Dissociative Photodetachment Dynamics

In this section, we address the DPD of $HOCO^-$ and the branching between stable HOCO radical and the OH + CO and H + CO_2 product channels. As shown in Fig. 1, at a photon energy of 3.20 eV, both the OH + CO (entrance) and H + CO_2 (exit) channel asymptotes are accessible. Fig. 6 shows the total photoelectron spectrum (electrons in coincidence with dissociative products *and* stable HOCO radicals). Note that owing to the higher photon energy, the vibrationally resolved features seen near the photodetachment threshold in Fig. 4 are no longer resolvable, and the very large vibrational density of states accessed at lower eKE using a 3.20 eV photon energy precludes vibrational resolution. The broad extent (1.5 eV) of the Franck-Condon region, arising from the geometry change between the anion and the neutral radical, has been confirmed by recent wavepacket dynamics calculations.[101, 107, 108] Separating the recorded photoelectrons by the identity of the photofragment

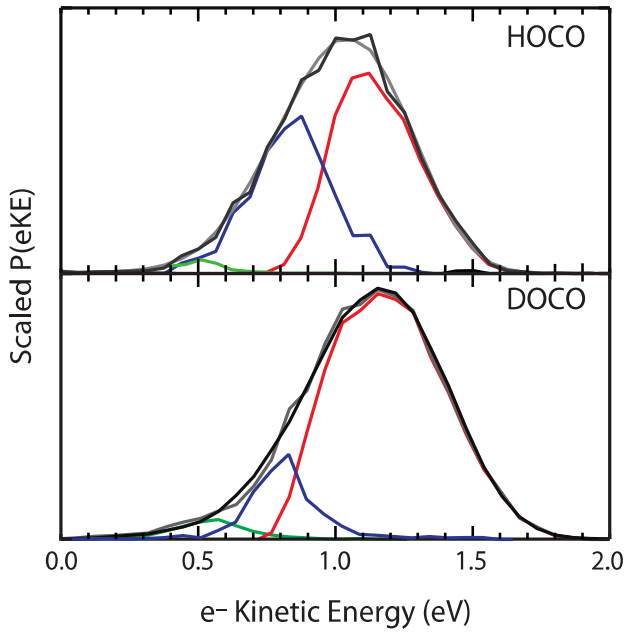

Fig. 6 Channel-resolved photoelectron spectra for HOCO (top) and DOCO (bottom). Photoelectrons from events leading to OH + CO dissociation are in green, those from H + CO_2 dissociation are blue, and photodetachment to stable HOCO is red. The sum of the three spectra is shown in black, and the experimental spectrum for all electrons is in gray.

yields channel-resolved photoelectron spectra as shown in Fig. 6, information not accessible in a conventional photodetachment experiment where only the photoelectron is detected. Each channel dominates in a specific region of eKE, corresponding to different internal energies in the nascent HOCO radical induced by the photodetachment process. The calculated barriers from the PESs in Table 1 predict ranges of eKE where these processes

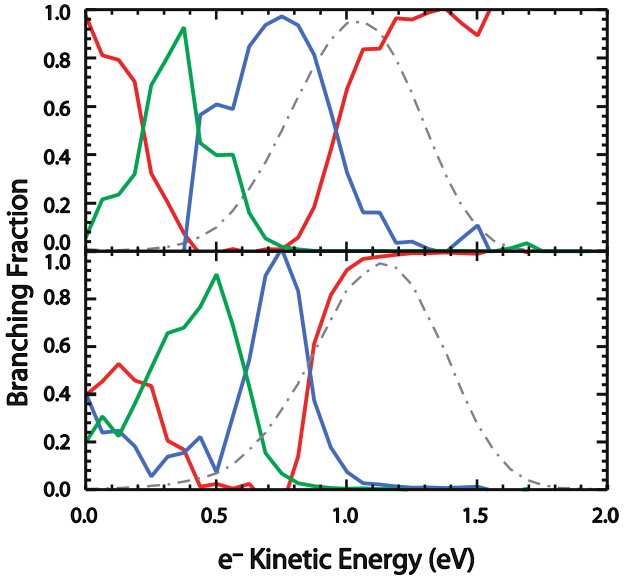

Fig. 7 Branching fractions for the three product channels as a function of eKE for HOCO (top) and DOCO (bottom). Each curve represents the fraction of events at that energy in each product channel using the color scheme of Fig. 6, with the total photoelectron spectra shown as the gray dashed lines.

should occur. While dissociation to OH + CO occurs in the expected energetic range (<0.69 eV), dissociation to H + CO_2 is observed with eKE much higher than the predicted limit of 0.61 eV, corresponding to dissociation below the calculated barrier. This is consistent with previous results from Lu *et al.*,[93] carrying out PPC experiments without the cryogenic EIBT, however it was clear in those experiments that significant internal energy (> 0.5 eV) was present in the precursor anions, as will be further discussed below. Interpretation of these new results as tunneling through the barrier to H + CO_2 is unambiguous due to the removal of uncertainty in the anion precursor internal energy.

Fitting each of these channel-resolved photoelectron spectra to the total photoelectron spectra for *all* events (stable radicals and both dissociation channels) for HOCO and DOCO allowed determination of the energy-resolved branching fractions in Fig. 7. This provides a direct measure of the fraction of events at a given eKE (and thus internal energy on the HOCO PES) that result in each final state (stable radicals or the OH + CO and H + CO_2 asymptotes). These branching fractions show that each channel dominates in a specific internal energy range, but there are discrete regions of energy where competition between channels occurs. These regions of competition hold crucial information that will be discussed in detail in the ensuing sections. Photodetachment to stable HOCO has already been discussed above, so we next turn our attention to the OH + CO channel.

The OH + CO Channel

A more complete understanding of the DPD dynamics can be obtained by analysis of the PPC spectra. These spectra are two-dimensional histograms of events with a given eKE and fragment KER in coincidence, and generally display diagonal features corresponding to conservation of total translational energy (E_{TOT} = eKE + KER). The maximum expected E_{TOT} can be predicted from a combination of AEAs and the relative energies of the dissociation asymptotes. Events occurring below this maximum E_{TOT} signifies partitioning of energy into internal degrees of freedom in the products, where $E_{int} = E_{TOT,max} - E_{TOT}$.

Coincidence spectra are shown for the OH + CO channel in Fig. 8, as observed in the "hot"[93] and "cold" experiments.[109] The diagonal lines mark the maximum E_{TOT} expected for *trans* (solid) and *cis* (dashed) isomers. Horizontal lines indicate the maximum allowed eKE for dissociation over the barrier to OH + CO from *trans*- and *cis*-HOCO. While the "hot" spectrum contains a significant amount of signal beyond these energetic limits, the "cold" spectrum is a narrow diagonal band with essentially all signal below the E_{TOT} limits. The OH + CO channel shows the most drastic changes due to cooling showing that > 0.5 eV of extra energy distributed in a non-Boltzmann fashion was contained in some of the hot anion precursors.

It is interesting to note that despite the fact that the beam population is ~96% *cis* isomers, the bulk of the signal in the lower (cold) frame of Fig. 8 lies *below* the limit for dissociation over the *cis* transition state to OH + CO products. Given the small fraction observed for trans-$HOCO^-$ (~4%) it is likely that at these energies dissociation occurs through a *cis*/*trans* isomerization pathway, discussed further below.

The OH + CO channel provides quantitative information about the energetics of the HOCO PES. As the entrance channel of the reaction, it is of critical importance, and an understanding of its role in DPD will help to connect this work to the overall reaction dynamics. It is immediately clear that no vibration is present in either fragment, consistent with collisions between vibrationally cold OH and CO. Analysis of the single diagonal band shows a FWHM of 0.08 eV in the total kinetic energy spectrum setting an upper limit to the internal energy of the anions, or conversely to the internal energy of the OH and CO products. This feature can be fit to a two- component Boltzmann rotational distribution, assuming equipartition of energy between the fragments with $B_e(OH)$ = 18.9 cm^{-1} and $B_e(CO)$ = 1.93 cm^{-1},[110,111] to find an upper limit of 250 K to the internal temperature of the products. The actual value is likely significantly smaller due to the

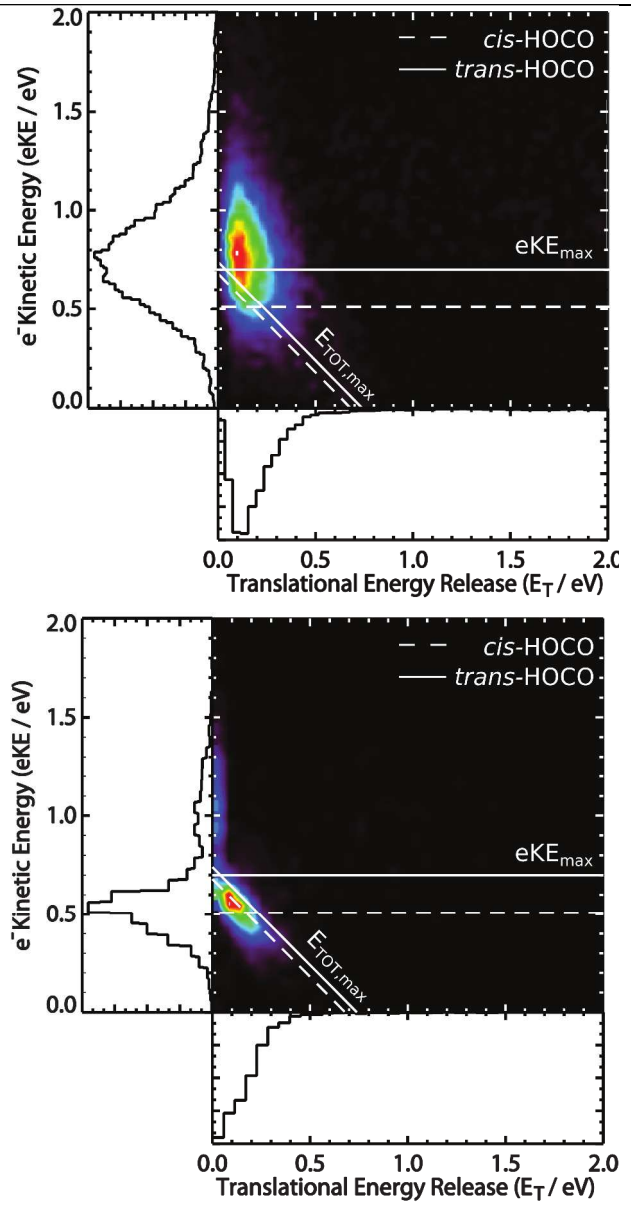

Fig. 8 PPC spectra for the OH + CO channel with "hot" anions (top) and "cold" anions (bottom). The diagonal lines mark the maximum E_{TOT} expected for *trans* and *cis* isomers. Horizontal lines indicate the maximum allowed eKE for dissociation over the barrier to OH + CO from *trans*- and *cis*-HOCO. In the "cold" spectrum the minor signal at E_T ~ 0 and eKE > 0.8 eV results from false coincidences with stable HOCO radicals.

contribution of the experimental resolution and ion internal temperature to the overall width. The diagonal feature is peaked very close to zero KER, implying either that in the Franck-Condon region of the anion, the neutral PES is very flat or that DPD is a sequential barrierless unimolecular decomposition. There is a significant geometry change upon photodetachment related to this dissociation pathway, as the anionic central OC bond length is 0.2 Å longer than the neutral,[62] with OH and CO equilibrium bond lengths closer to those of the free diatomic molecules.

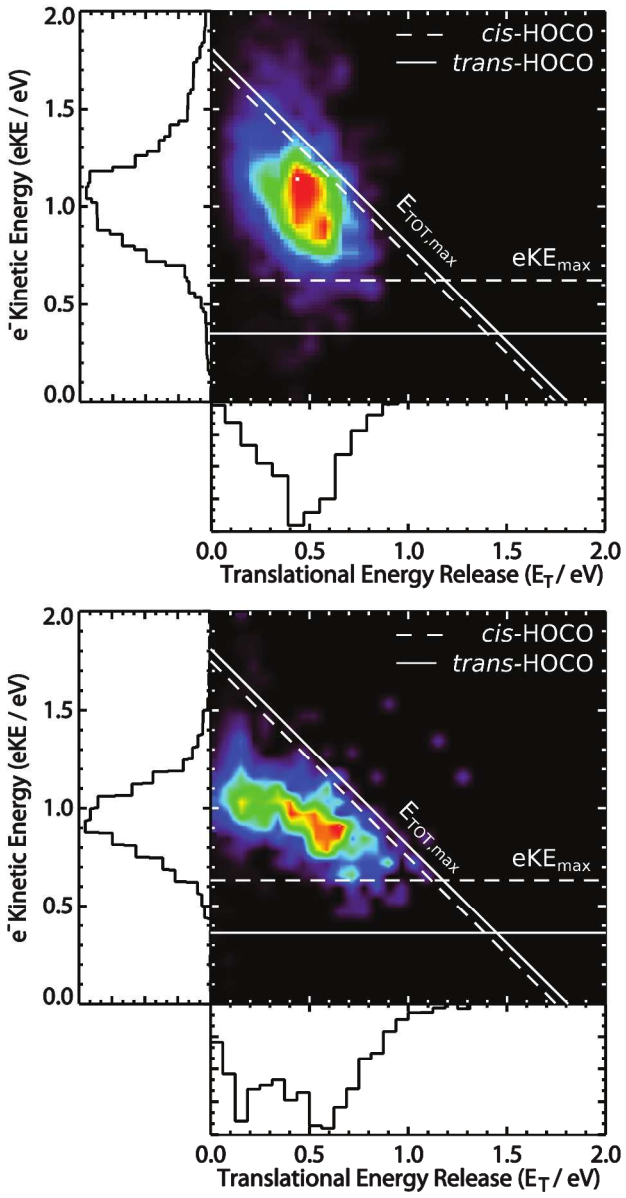

Fig. 9 PPC spectra for dissociation to H + CO_2. Again, the top spectrum is "hot" and the bottom is "cold" as in Figure 8. The diagonal lines mark the maximum E_{tot} expected for trans and cis isomers. Horizontal lines indicate the maximum allowed eKE for dissociation over the barrier to H + CO_2 from *trans*- and *cis*-HOCO.

The narrow internal energy distribution in the OH + CO products and the new and more accurate determinations of the electron affinities for *cis*- and *trans*-HOCO allow the well depths for the two isomers to be accurately determined. Energy conservation in the DPD process gives $D_0 = h\nu - AEA - E_{TOT}$, yielding a well depth for *cis*-HOCO of 0.99 ± 0.02 eV, supported by the HEAT345-(Q) value of 1.01 eV. Given these values for the *cis* isomer, the trans well depth is then experimentally estimated to be 1.07 ± 0.02 eV, with HEAT345-(Q) giving 1.08 eV. These results fall well within the upper limit for D_0 obtained in photoionization experiments by Ruscic *et al.* of 1.25 eV.

The H + CO_2 Channel

Coincidence spectra for the "hot" and "cold" experiment are given for the H + CO_2 channel in Fig. 9. The diagonal lines mark the maximum E_{TOT} expected for *trans* (solid) and *cis* (dashed) isomers. Horizontal lines indicate the maximum allowed eKE for dissociation over the barrier to H + CO_2 from *trans*- and *cis*-HOCO. It is clear that in both the "hot" (top) and "cold" (bottom) spectra, essentially all signal is above these eKE limits, implying that either dissociation to H + CO_2 occurs below the barrier, or the calculated barrier heights are not correct. It is also apparent that the "cold" data is shifted to lower eKE by ~0.2 eV, reflecting the reduction in the anion internal energy distribution. Beyond purely energetic evidence from the photoelectron spectra, the branching fractions and coincidence spectra also show characteristic signs of tunneling, in particular the large energy range over which competition between stable radicals and H + CO_2 products occurs as shown in Fig. 7 and the characteristic shape of the coincidence spectrum with the KER degraded to lower values as eKE increases in the lower frame of Fig. 9. These results for both HOCO and DOCO were discussed in some detail in ref. 6.

The role of a tunneling mechanism for production of H + CO_2 has been debated in different studies.[11-17, 21] In the DPD studies on cold $HOCO^-$ anions, the experimental energetics show that *all* H + CO_2 products result from tunneling. It is particularly interesting to examine the branching fractions shown in Fig. 7 over the eKE range from 0.75 – 1.3 eV in HOCO and 0.75 – 1.2 eV in DOCO where competition between tunneling to H + CO_2 and stable radicals is observed. In these ranges the competition arises as tunneling lifetimes approach the total time-of-flight of dissociation fragments to the neutral detector, resulting in a number of energized HOCO products reaching the detector before dissociation by tunneling. Under the conditions of these experiments, this indicates that tunneling occurs over the whole range up to the 7.8 μs flight time from the interaction region to the neutral particle detector. These long tunneling lifetimes are not surprising as these events occur 0.5 - 0.7 eV below the lowest calculated barrier, for *cis*-HOCO → H + CO_2. A parameterized model barrier was optimized to fit these observed tunneling lifetimes, allowing direct extraction of a realistic one-dimensional potential that reproduces many of the observables in these DPD experiments.[6]

This model assumed that only motion along the OH bond contributes to tunneling dissociation, and that internal energy is not necessarily statistically distributed among the six normal modes. A model potential barrier was generated from an avoided crossing between a Morse oscillator dissociating to the first

excited state of neutral CO_2, and a direct repulsive curve asymptotically approaching the energy of isolated H and CO_2 products. Experimental tunneling rates were extracted by inverting the fraction of H + CO_2 products observed in the energy range where competition with stable HOCO was observed, using the number of classical OH oscillations occurring during the total time-of-flight to the detector. These experimental tunneling coefficients, now determined as a function of internal energy in the HOCO neutral, were then directly compared to tunneling coefficients for the model barrier, calculated using the WKB approximation. The final element of this model deals with the fact that not all internal energy promotes tunneling, therefore the energy in the OH bond coordinate was approximated by the total energy in the "OH stretching" normal mode, plus a fraction of the energy contained in the rest of the normal modes. With this simple quasi one-dimensional model, the parameters determining barrier and the energy fraction in the OH bond as well as the fraction of the energy balance promoting dissociation were iteratively optimized to best reproduce the experimental data simultaneously for HOCO and DOCO.

The optimized barrier, shown in Fig. 10, reproduces all observed tunneling coefficients well with the assumption that tunneling for HOCO required one quantum in the H-O stretch, DOCO required two quanta in the D-O stretch, and a fraction χ = 0.19 of the excess internal energy promoted tunneling. More importantly, the model barrier can be used, through comparison with *ab initio* calculations, to predict CO_2 product internal energy distributions that can be compared to those measured in the DPD experiments. The optimized results indicate that up to 0.4 eV of the internal energy is in "non-dissociative" vibrational modes at the moment of the tunneling event, which within the approximations of the model would be reflected as internal energy in the CO_2 product. This range spans the observed product internal energy of 0.2-0.3 eV in the coincidence spectra, taken as the difference between the maximum E_{TOT} expected and the maximum in signal intensity along the diagonal of the PPC spectrum in Fig. 9. Further agreement is found when comparing the model barrier to a "minimum-energy" barrier constructed from a fully relaxed scan of the change in electronic energy (CCSD/aug-cc-pVTZ) as a function of H-O bond stretching, also shown in Fig. 10. As shown in ref. 6 a two-dimensional slice along the r_{OH} and θ_{OCO} coordinates of the PES reveals that the minimum-energy pathway is strongly curved at the transition state in this plane, and thus the horizontal tunneling pathway cannot follow the minimum-energy pathway. Therefore, the difference in energy between the optimized barrier and the minimum-energy barrier in the exit channel, also found to be ~0.3 eV, can be thought of as the non-dissociative internal energy contribution to the one-dimensional surface, reproducing the experimental data.

This quasi-one-dimensional semi-empirical model has a number of significant approximations, but it unambiguously demonstrates that the data observed for the competition between stable radicals and dissociation to H/D + CO_2 in the PPC experiments are consistent with 'deep tunneling' through the barrier on a timescale of several microseconds. Quantum dynamics studies of the DPD of $HOCO^-$ using the older LTSH surface indicated no role for tunneling at these energies,[112] but

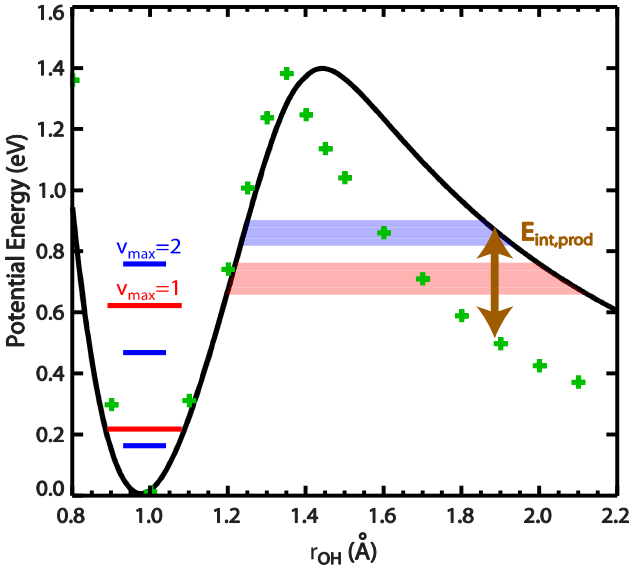

Fig. 10 The extracted barrier for tunneling to H/D + CO_2 based on the studies of HOCO and DOCO (black line). Also shown is the minimum-energy surface computed at the CCSD/aug-cc-pVTZ level (green symbols). The range of energies where tunneling data was available is shaded for HOCO (red) and DOCO (blue). Within the approximations of the model, the difference between the minimum-energy surface and the extracted surface reflects the internal energy stored in the product CO_2. Reprinted with permission from ref. 6. Copyright 2011, AIP Publishing LLC.

that has been shown to be a result of the barrier on that surface being far too thick.[59] These experimental results have been complemented by a number of recent theoretical studies. Stanton, Barker and co-workers used high-level *ab initio* calculations of the stationary points on the HOCO PES to carry out semiclassical transition state theory calculations of the reaction rate coefficients, and found evidence that at room temperature up to 85% of the reactive flux to H + CO_2 products resulted from tunneling.[57] Guo and co-workers performed a five-dimensional quantum wavepacket dynamics study that found resonances in the HOCO well that promoted tunneling to H + CO_2, as well as capturing aspects of the branching towards OH + CO products.[108] In more recent work, they have shown that exact 6-D quantum wavepacket simulations are possible on the picosecond time-scale. There is no prospect of propagating the solutions on the microsecond tunneling time scale indicated by the observed branching between stable HOCO radical and H + CO_2 products. However, Guo and co-workers found strong mode specificity for tunneling lifetimes over several orders of magnitude using an approximate method, the Sudden Vector Projection model.[101] Bowman and co-workers have also examined this problem using an alternate projection theory approach for combination states of the OCO bend and the CO stretch, finding tunneling rates generally consistent with the experimental results.[113] Finally, Wagner and co-workers have recently applied more formally the quasi-one-dimensional treatment developed to model the present experiments for several HOCO PESs as well as a number of distinct approaches to calculating the deep tunneling rate yielding H + CO_2 products.[114] These recent theoretical advances in concert with the

experimental measurements on deep tunneling show how HOCO and the OH + CO → H + CO_2 reaction are becoming benchmarks for elementary complex-forming reactions.

Channel Competition

Interestingly, as noted above, most of the dissociation to OH + CO found in these experiments occurs from detachment to HOCO with internal energy below the barrier for dissociation of *cis*-HOCO to OH + CO but above that for *trans*-HOCO. This region of the PES is shown in Fig. 11, including the pathways considered below. Given that the composition of the beam is predominantly *cis*-$HOCO^-$, two possible explanations for this observation arise. The first is that dissociation to OH + CO in this internal energy range proceeds exclusively from the small percentage of *trans*-$HOCO^-$. The second is that neutrals that are initially cis first isomerize to *trans*-HOCO prior to dissociation. Regarding the first explanation, even with unity efficiency of the reaction *trans*-$HOCO^-$ + hν (3.20 eV) → OH + CO + e^-, the yield of OH + CO products in this energy range is too large for this to be the sole mechanism. The energy-resolved branching fractions for DPD of HOCO show that below the *cis*-HOCO → OH + CO barrier there is competition between the OH + CO and H + CO_2 channels, leading to roughly equal amounts of each product in this energy range. However, above the barrier from *cis*-HOCO to OH + CO, the only product observed is OH + CO, implying that, when that channel is open, this dissociation is significantly faster than dissociation to H + CO_2. These observations are consistent with the second explanation, where the process of isomerization from *cis*- to *trans*-HOCO occurs at a rate similar to tunneling to H + CO_2, and dissociation of *trans*-HOCO to OH + CO occurs promptly. This argument is further reinforced by the observation that this region of competition is not present in DOCO, where all events in this energy range lead to dissociation to OD + CO. As shown in Fig. 1, in the deuterated case the isomerization and OD + CO barriers all shift to lower energy due to the reduction in zero-point energy upon deuteration, while the barrier to D + CO_2 remains essentially constant due to the OD stretch being the reaction coordinate. This shift in relative energies is more than sufficient to explain the loss of the competition feature, as the lifetimes for D + CO_2 production are significantly longer and thus the isomerization mechanism is dominant. In the current experiments, some contribution from other mechanisms cannot be conclusively ruled out, and it remains possible that some events originate from *trans*-HOCO anions. If this is the case, then the noted competition must arise from a purely coincidental balance of prompt dissociation to OH + CO from *trans*-HOCO and relatively slow tunneling from *cis*-HOCO to H + CO_2.

The mechanism behind the proposed isomerization requires additional consideration. The lowest-lying isomerization transition state is out-of-plane (τ-TS in Fig. 1),[59] and the energy of 0.29 eV implies at least four quanta in the torsional mode are required to cross it (assuming no coupling with in-plane vibrational modes). However, since both the anion and neutral for both isomers are planar, no torsional excitation is expected upon photodetachment. Thus a mechanism to redistribute energy from modes with planar symmetry to out-of-plane modes (forbidden in the harmonic approximation) is required, or a higher-lying planar isomerization transition state through which the system can pass without torsional motion must exist. Accurately calculating

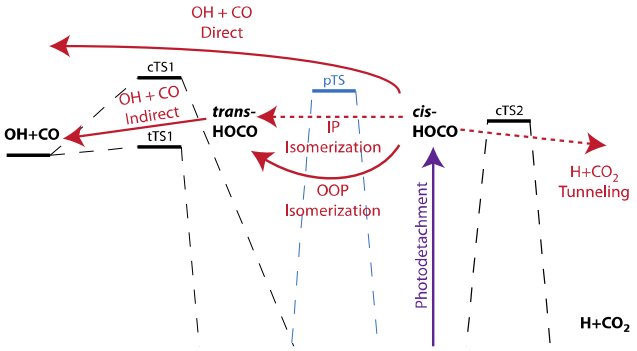

Fig. 11 Diagram of possible dissociation processes occurring in the energy range where the OH + CO channel is allowed. Photodetachment of *cis*-$HOCO^-$ leads to excitation high in the *cis*-HOCO well. When energetically allowed, dissociation directly to OH + CO over the cTS1 barrier is dominant, despite the H + CO_2 channel being energetically favored. Below the cTS1 barrier, dissociation to OH + CO occurs through a two-step mechanism that first involves in-plane (IP) or out-of-plane (OOP) isomerization to *trans*-HOCO by an as-yet-unknown mechanism. Surprisingly, this process competes with direct dissociation (or fast tunneling) to H + CO_2.

energy transfer from planar to torsional modes are quite difficult without detailed experimental data,[115] so the out-of-plane isomerization process, while possible, has not been explored further to date.

The case of planar isomerization is only slightly simpler. No first-order stationary point corresponding to this process has been located on the various high-level HOCO PESs. Lower-level CCSD/aug-cc-pVTZ calculations[116] were carried out in this laboratory, yielding a second-order stationary point with imaginary frequencies in both the torsional and HOC wagging modes. The energy of this transition state falls near the proposed isomerization range between the *cis*- and *trans*-TS1 energies, suggesting that more sophisticated calculations may show that this process is energetically allowed.

If this transition state is not found to be low enough for planar isomerization to be energetically allowed, it may also be possible that tunneling plays a role here as well. A simple analysis similar to that for dissociation to H + CO_2 has been performed, though here the barrier is assumed to be an Eckart potential which is known to be a reasonable approximation for many molecular processes.[117] Tunneling coefficients for the Eckart barrier lead to a tunneling rate of 1.5×10^{-6} s^{-1}; quite low, but this process needs only to be competitive with tunneling to H + CO_2 to be active. At these energies, the tunneling lifetime (1/e) to H + CO_2 is approximately 100 ps. For isomerization, the most directly active normal mode of *cis*-HOCO is the HOC bend, with a fundamental frequency of 38 THz (1272 cm^{-1}).[101] From this, the lifetime for tunneling to *trans*-HOCO of 18 ns is found, significantly higher than the predicted H + CO_2 lifetime. However, more sophisticated calculations may reduce the energy of this transition state, thus reducing the lifetime and making this process more competitive.

Excited State Dissociation Dynamics

The PPC studies discussed above all refer to dissociation

dynamics on the ground state of the HOCO radical. However, in the earlier study at a photon energy of 4.80 eV, a high translational energy dissociation channel with ~0.2 eV of product internal excitation was observed at ~1.9 eV above the OH + CO dissociation asymptote.[62] This feature is characteristic of direct DPD on a repulsive PES. The low-lying excited states of *cis*- and *trans*-HOCO have been investigated theoretically by Li and Francisco.[54] They reported the detailed behaviour of the excited states for *trans*-HOCO. In particular for this isomer, they found the $1^2A''$ excited state to be repulsive beyond 1.5 Å in the central HO-CO bond. Assuming, as Li and Francisco reported, that the *cis*-HOCO PES was very similar, photodetachment to this low-lying excited state would be expected to lead to dissociation to OH + CO over a significant fraction of the Franck-Condon region, given the calculated central O-C bond lengths of 1.52 Å for the ground state *trans*-$HOCO^-$ anion[64] and 1.46 Å for the *cis*-$HOCO^-$ anion.[41]

An alternative approach to the investigation of the low-lying electronic states of HOCO is by charge exchange neutralization of $HOCO^+$. Charge exchange between *trans*-$HOCO^+$ and caesium is energetically nearly resonant for production of the excited $1^2A''$ state of *trans*-HOCO. In addition there is excellent Franck-Condon overlap between the anion and the neutral excited state, as shown by the similar geometries calculated for the cation and the excited state.[92] The experiments found that charge exchange led entirely to dissociation, with product yields showing a 3:1 preference for OH + CO over H + CO_2. As noted with respect to the PPC experiments, the $1^2A''$ diabatic state directly dissociates to OH + CO products, consistent with the experimental observations. However, in charge exchange the nascent neutral HOCO is produced at much shorter central HO-CO bond lengths (1.23 Å in *trans*-$HOCO^+$ vs. 1.46 Å for *cis*-$HOCO^-$), and thus much higher potential energies, promoting the dissociation to H + CO_2 not seen in the PPC experiments. Li and Francisco found that the $1^2A''$ state is bound with respect to dissociation to H + CO_2. Therefore, it was proposed that dissociation to this channel occurs by rapid predissociation from $1^2A''$ to the $2^2A'$ state followed by nonadiabatic coupling to the dissociative region of the $1^2A'$ ground state. Interestingly, the $2^2A'$ state is essentially the upper state in the two-state model employed for extraction of the barrier to H + CO_2 discussed earlier. Further characterization of this process could yield significant insights into the excited state dynamics of HOCO.

Outstanding Questions

The recent experimental and theoretical studies of HOCO and the OH + CO → H + CO_2 reaction reviewed here represent a significant expansion of the knowledge of the detailed dynamics on the HOCO PES, however, significant questions remain. The experimental results suggest that *cis*-*trans* isomerization in the HOCO well plays an important role in modulating OH + CO and H + CO_2 branching ratios at energies near the threshold for H + CO_2 formation. Further theoretical examination of this process would be valuable as the effects may be more complex than the low out-of-plane torsional transition state between the two isomers implies.

The observations presented here also need to be connected to studies of other regions on the 6-dimensional HOCO PES. Previous studies[90, 91] have shown that photodetachment of the formate anion (HCO_2^-) accesses a local minimum (the formyloxyl radical, HCO_2) in the region of the HOCO PES reached following isomerization of the *trans*-HOCO radical over the higher energy barrier tTS4 (Fig. 1). PPC experiments have shown that the rapid predissociation of HCO_2 leads to high levels of CO_2 bend excitation, in contrast to quantum dynamics studies on the LTSH PES.[101] As discussed above, the LTSH PES also does not support the deep tunneling observed in the *cis*-HOCO → H + CO_2 dissociation. Thus, it will be of great interest to examine the performance of the new global PESs available for HOCO for reproducing the dynamics on this different region of the potential energy surface.

An important element of future experimental studies using the PPC technique will be modulation of the populations of the two isomers in the beam. Isomer-resolved experiments will help to further isolate the elements of the overall dissociation dynamics that occur in the *cis* or *trans* regions of the PES, and the degree to which isomerization between them plays an important role in these DPD experiments. We have now demonstrated methods for preparing vibrationally excited anions prior to injection into the EIBT,[118] opening the way to examining the effects of selective vibrational excitation and intramolecular vibrational redistribution on the reaction dynamics in this system. Given the predominant formation of *cis*-$HOCO^-$ in the ion source, investigation of overtone excitation as a route to promoting isomerization to *trans*-$HOCO^-$ or isomerization to the much more stable formate anion will be the focus of initial efforts. In *cis*-HOCO, examining the effects of vibrational excitation directly in the H-O stretch (essentially the reaction coordinate for tunneling to H + CO_2) as well as overtones of the central O-C stretch will be of greatest interest as we further investigate the reaction dynamics of the HOCO system by photodetachment of $HOCO^-$.

Conclusions

The HOCO radical has proven to be more than an important reaction intermediate in atmospheric and combustion processes – it is also a rich and complex chemical physics problem and underscores the significance of OH + CO ⟶ H + CO_2 as a prototypical complex-forming elementary reaction.[1] The photodetachment and DPD experiments described here, along with recent theoretical advances, have begun to resolve the dynamics occurring on the PES of the OH + CO reaction as a function of energy but are by no means complete. The PPC experiments serve as crucial benchmarks for theoretical reaction dynamics studies of this system, providing quantitative, microcanonical results such as energy-resolved branching fractions and tunneling rates, vibrational frequencies, electron affinities and well depths. In addition, these experimental observations have identified new puzzles such as the role of *cis*-*trans* isomerization in the modulation of OH + CO versus H + CO_2 product channels, and a strong photodetachment resonance more than 0.1 eV above the detachment threshold, each meriting further study. With significant outstanding questions and new experimental capabilities continuously in development, it is clear that the HOCO system will remain a fertile ground for fundamental studies of elementary chemical reactions.

Notes and references

B.L.J.P. Poad, B.B. Shen and A. Ray are acknowledged for their contributions to the experiments. In addition, we acknowledge discussions with J. Stanton A. Wagner, H. Guo, J.M. Bowman and T.L. Nguyen. This material is based upon work supported by the U.S. Department of Energy Office of Science, Office of Basic Energy Sciences under Award Number DE-FG03-98ER14879.

[a] *Department of Physics, University of California, San Diego, 9500 Gilman Drive, La Jolla, CA 92093-0340.; current address: Department of Chemistry, Stony Brook University, Stony Brook, NY 11794*
[b] *Department of Chemistry and Biochemistry, University of California, San Diego, 9500 Gilman Drive, La Jolla CA 92093-0340. Fax: 858-534-9856; Tel: 858-534-5559; E-mail: rcontinetti@ucsd.edu*

1. H. Guo, *Int. Rev. Phys. Chem.*, 2012, 31, 1-68.
2. J. A. Miller, R. J. Kee and C. K. Westbrook, *Ann. Rev. Phys. Chem.*, 1990, 41, 345-387.
3. T. Rockmann, C. E. M. Brenninkmeijer, G. Saueressig, P. Bergamaschi, J. N. Crowley, H. Fischer and P. J. Crutzen, *Science*, 1998, 281, 544-546.
4. J. S. Francisco, J. T. Muckerman and H.-G. Yu, *Acc. Chem. Res.*, 2010, 43, 1519-1526.
5. J. W. Stock, C. S. Boxe, R. Lehmann, J. L. Grenfell, A. B. C. Patzer, H. Rauer and Y. L. Yung, *Icarus*, 2012, 219, 13-24.
6. C. J. Johnson, B. L. J. Poad, B. B. Shen and R. E. Continetti, *J. Chem. Phys.*, 2011, 134, 171106.
7. C. J. Johnson, M. E. Harding, B. L. J. Poad, J. F. Stanton and R. E. Continetti, *J. Am. Chem. Soc.*, 2011, 133, 19606-19609.
8. I. W. M. Smith and R. Zellner, *J. Chem. Soc., Farad. Trans. II*, 1973, 69, 1617 - 1627.
9. G. Paraskevopoulos and R. S. Irwin, *Chem. Phys. Lett.*, 1982, 93, 138-143.
10. G. Paraskevopoulos and R. S. Irwin, *J. Chem. Phys.*, 1984, 80, 259-266.
11. M. J. Frost, P. Sharkey and I. W. M. Smith, *Farad. Disc.*, 1991, 91, 305-317.
12. M. J. Frost, P. Sharkey and I. W. M. Smith, *J. Phys. Chem.*, 1993, 97, 12254-12259.
13. D. Fulle, H. F. Hamann, H. Hippler and J. Troe, *J. Chem. Phys.*, 1996, 105, 983-1000.
14. D. M. Golden, G. P. Smith, A. B. McEwen, C. L. Yu, B. Eiteneer, M. Frenklach, G. L. Vaghjiani, A. R. Ravishankara and F. P. Tully, *J. Phys. Chem. A*, 1998, 102, 8598-8606.
15. R. S. Zhu, E. G. W. Diau, M. C. Lin and A. M. Mebel, *J. Phys. Chem. A*, 2001, 105, 11249-11259.
16. J. P. Senosiain, C. B. Musgrave and D. M. Golden, *Int. J. Chem. Kin.*, 2003, 35, 464-474.
17. J. P. Senosiain, S. J. Klippenstein and J. A. Miller, *Proc. Comb. Inst.*, 2005, 30, 945-953.
18. W. C. Chen and R. A. Marcus, *J. Chem. Phys.*, 2005, 123, 094307.
19. M. C. van Beek, K. Schreel and J. J. ter Meulen, *J. Chem. Phys.*, 1998, 109, 1302-1309.
20. D. M. Sonnenfroh, R. G. Macdonald and K. Liu, *J. Chem. Phys.*, 1991, 94, 6508-6518.
21. M. Alagia, N. Balucani, P. Casavecchia, D. Stranges and G. G. Volpi, *J. Chem. Phys.*, 1993, 98, 8341-8344.
22. C. Y. Shi, L. Ren and F. N. Kong, *Chemphyschem*, 2006, 7, 820-823.
23. N. F. Scherer, C. Sipes, R. B. Bernstein and A. H. Zewail, *J. Chem. Phys.*, 1990, 92, 5239-5259.
24. S. K. Shin, C. Wittig and W. A. Goddard, *J. Phys. Chem.*, 1991, 95, 8048-8053.
25. S. I. Ionov, G. A. Brucker, C. Jaques, L. Valachovic and C. Wittig, *J. Chem. Phys.*, 1993, 99, 6553-6561.
26. G. W. Flynn and R. E. Weston, *J. Phys. Chem.*, 1993, 97, 8116-8127.
27. M. Brouard, I. Burak, D. W. Hughes, K. S. Kalogerakis, J. P. Simons and V. Stavros, *J. Chem. Phys.*, 2000, 113, 3173-3180.
28. D. E. Milligan and M. E. Jacox, *J. Chem. Phys.*, 1971, 54, 927-942.
29. M. E. Jacox, *J. Chem. Phys.*, 1988, 88, 4598-4607.
30. D. Forney, M. E. Jacox and W. E. Thompson, *J. Chem. Phys.*, 2003, 119, 10814-10823.
31. T. J. Sears, W. M. Fawzy and P. M. Johnson, *J. Chem. Phys.*, 1992, 97, 3996-4007.
32. J. T. Petty and C. B. Moore, *J. Mol. Spec.*, 1993, 161, 149-156.
33. J. T. Petty and C. B. Moore, *J. Chem. Phys.*, 1993, 99, 47-55.
34. A. Miyoshi, H. Matsui and N. Washida, *J. Chem. Phys.*, 1994, 100, 3532-3539.
35. H. E. Radford, W. Wei and T. J. Sears, *J. Chem. Phys.*, 1992, 97, 3989-3995.
36. T. J. Sears, H. E. Radford and M. A. Moore, *J. Chem. Phys.*, 1993, 98, 6624-6631.
37. H. E. Radford, M. A. Moore, T. J. Sears, J. Grussdorf, J. Nolte and F. Temps, *J. Mol. Spec.*, 1994, 165, 137-149.
38. T. Oyama, W. Funato, Y. Sumiyoshi and Y. Endo, *J. Chem. Phys.*, 2011, 134, 174303.
39. C.-H. Chang, G. T. Buckingham and D. J. Nesbitt, *J. Phys. Chem. A*, 2013, 117, 13255-13264.
40. R. C. Fortenberry, X.-C. Huang, J. S. Francisco, T. D. Crawford and T. J. Lee, *J. Chem. Phys.*, 2011, 135, 134301.
41. R. C. Fortenberry, X.-C. Huang, J. S. Francisco, T. D. Crawford and T. J. Lee, *J. Chem. Phys.*, 2011, 135, 214303.
42. M. Mladenovic, *J. Chem. Phys.*, 2012, 137, 014306.
43. M. Mladenovic, *J. Phys. Chem. A*, 2013, 117, 7224-7235.
44. X.-C. Huang, R. C. Fortenberry, Y. Wang, J. S. Francisco, T. D. Crawford, J. M. Bowman and T. J. Lee, *J. Phys. Chem. A*, 2013, 117, 6932-6939.
45. A. D. McLean and Y. Ellinger, *Chem. Phys. Lett.*, 1983, 98, 450-453.
46. A. D. McLean and Y. Ellinger, *Chem. Phys.*, 1985, 94, 25-41.
47. T. V. Duncan and C. E. Miller, *J. Chem. Phys.*, 2000, 113, 5138-5140.
48. G. C. Schatz, M. S. Fitzcharles and L. B. Harding, *Farad. Disc.*, 1987, 84, 359-369.
49. K. Kudla, G. C. Schatz and A. F. Wagner, *J. Chem. Phys.*, 1991, 95, 1635-1647.
50. K. S. Bradley and G. C. Schatz, *J. Chem. Phys.*, 1997, 106, 8464-8472.
51. H. G. Yu, J. T. Muckerman and T. J. Sears, *Chem. Phys. Lett.*, 2001, 349, 547-554.
52. M. J. Lakin, D. Troya, G. C. Schatz and L. B. Harding, *J. Chem. Phys.*, 2003, 119, 5848-5859.
53. M. Aoyagi and S. Kato, *J. Chem. Phys.*, 1988, 88, 6409-6418.
54. Y. M. Li and J. S. Francisco, *J. Chem. Phys.*, 2000, 113, 7963-7970.
55. R. Valero, M. C. van Hemert and G. J. Kroes, *Chem. Phys. Lett.*, 2004, 393, 236-244.
56. X. Song, J. Li, H. Hou and B. Wang, *J. Chem. Phys.*, 2006, 125, 094301.
57. T. L. Nguyen, B. C. Xue, R. E. Weston, J. R. Barker and J. F. Stanton, *J. Phys. Chem. Lett.*, 2012, 3, 1549-1553.
58. R. E. Weston, T. L. Nguyen, J. F. Stanton and J. R. Barker, *J. Phys. Chem. A*, 2013, 117, 821-835.
59. J. Li, Y. Wang, B. Jiang, J. Ma, R. Dawes, D. Xie, J. M. Bowman and H. Guo, *J. Chem. Phys.*, 2012, 136, 041103.
60. J. Li, C. Xie, J. Ma, Y. Wang, R. Dawes, D. Xie, J. M. Bowman and H. Guo, *J. Phys. Chem. A*, 2012, 116, 5057-5067.
61. J. Chen, X. Xu, X. Xu and D. H. Zhang, *J. Chem. Phys.*, 2013, 138, 221104.
62. T. G. Clements, R. E. Continetti and J. S. Francisco, *J. Chem. Phys.*, 2002, 117, 6478-6488.
63. J. R. Smith, J. B. Kim and W. C. Lineberger, *Phys. Rev. A*, 1997, 55, 2036-2043.
64. D. A. Dixon, D. Feller and J. S. Francisco, *J. Phys. Chem. A*, 2003, 107, 186-190.

65. B. Ruscic, A. F. Wagner, L. B. Harding, R. L. Asher, D. Feller, D. A. Dixon, K. A. Peterson, Y. Song, X. M. Qian, C. Y. Ng, et al., *J. Phys. Chem. A*, 2002, 106, 2727-2747.
66. D. Feller, D. A. Dixon and J. S. Francisco, *J. Phys. Chem. A*, 2003, 107, 1604-1617.
67. K. Kudla, A. G. Koures, L. B. Harding and G. C. Schatz, *J. Chem. Phys.*, 1992, 96, 7465-7473.
68. M. I. Lester, B. V. Pond, M. D. Marshall, D. T. Anderson, L. B. Harding and A. F. Wagner, *Farad. Disc.*, 2001, 118, 373-385.
69. M. E. Greenslade, M. Tsiouris, R. T. Bonn and M. I. Lester, *Chem. Phys. Lett.*, 2002, 354, 203-209.
70. M. D. Marshall, B. V. Pond and M. I. Lester, *J. Chem. Phys.*, 2003, 118, 1196-1205.
71. M. I. Lester, B. V. Pond, D. T. Anderson, L. B. Harding and A. F. Wagner, *J. Chem. Phys.*, 2000, 113, 9889-9892.
72. D. C. Clary and G. C. Schatz, *J. Chem. Phys.*, 1993, 99, 4578-4589.
73. H. K. Gerardi, A. F. DeBlase, X. Su, K. D. Jordan, A. B. McCoy and M. A. Johnson, *J. Phys. Chem. Lett.*, 2011, 2, 2437-2441.
74. E. M. Goldfield, S. K. Gray and G. C. Schatz, *J. Chem. Phys.*, 1995, 102, 8807-8817.
75. D. H. Zhang and J. Z. H. Zhang, *J. Chem. Phys.*, 1995, 103, 6512-6519.
76. F. N. Dzegilenko and J. M. Bowman, *J. Chem. Phys.*, 1996, 105, 2280-2286.
77. H. G. Yu and J. T. Muckerman, *J. Chem. Phys.*, 2002, 117, 11139-11145.
78. D. A. McCormack and G. J. Kroes, *Chem. Phys. Lett.*, 2003, 373, 648-649.
79. R. Valero, D. A. McCormack and G. J. Kroes, *J. Chem. Phys.*, 2004, 120, 4263-4272.
80. D. M. Medvedev, S. K. Gray, E. M. Goldfield, M. J. Lakin, D. Troya and G. C. Schatz, *J. Chem. Phys.*, 2004, 120, 1231-1238.
81. R. R. Bernecker and F. A. Long, *J. Phys. Chem.*, 1961, 65, 1565-1569.
82. M. A. Haney and J. L. Franklin, *Trans. Farad. Soc.*, 1969, 65, 1794-1804.
83. B. Ruscic, M. Schwarz and J. Berkowitz, *J. Chem. Phys.*, 1989, 91, 6780-6785.
84. B. Ruscic and M. Litorja, *Chem. Phys. Lett.*, 2000, 316, 45-50.
85. J. A. Burt, J. L. Dunn, M. J. McEwan, M. M. Sutton, A. E. Roche and H. I. Schiff, *J. Chem. Phys.*, 1970, 52, 6062-6075.
86. R. C. Fortenberry, X. Huang, J. S. Francisco, T. D. Crawford and T. J. Lee, *J. Chem. Phys.*, 2012, 136, 234309.
87. T. M. Miller, A. A. Viggiano, A. E. S. Miller, R. A. Morris, M. Henchman, J. F. Paulson and J. M. Vandoren, *J. Chem. Phys.*, 1994, 100, 5706-5714.
88. E. Garand, K. Klein, J. F. Stanton, J. Zhou, T. I. Yacovitch and D. M. Neumark, *J. Phys. Chem. A*, 2010, 114, 1374-1383.
89. E. H. Kim, S. E. Bradforth, D. W. Arnold, R. B. Metz and D. M. Neumark, *J. Chem. Phys.*, 1995, 103, 7801-7814.
90. T. G. Clements and R. E. Continetti, *J. Chem. Phys.*, 2001, 115, 5345-5348.
91. A. W. Ray, B. B. Shen, B. L. J. Poad and R. E. Continetti, *Chem. Phys. Lett.*, 2014, 592, 30-35.
92. J. D. Savee, J. E. Mann and R. E. Continetti, *J. Phys. Chem. A*, 2010, 114, 1485-1491.
93. Z. Lu, Q. Hu, J. E. Oakman and R. E. Continetti, *J. Chem. Phys.*, 2007, 126, 194305.
94. J. D. Savee, J. E. Mann, C. M. Laperle and R. E. Continetti, *Int. Rev. Phys. Chem.*, 2011, 30, 79-113.
95. R. E. Continetti, *Int. Rev. Phys. Chem.*, 1998, 17, 227-260.
96. K. A. Hanold, A. K. Luong, T. G. Clements and R. E. Continetti, *Rev. Sci. Instrum.*, 1999, 70, 2268-2276.
97. C. J. Johnson, B. B. Shen, B. L. J. Poad and R. E. Continetti, *Rev. Sci. Instrum.*, 2011, 82, 105105.
98. P. A. Schulz, R. D. Mead, P. L. Jones and W. C. Lineberger, *J. Chem. Phys.*, 1982, 77, 1153-1165.
99. F. Goldfarb, C. Drag, W. Chaibi, S. Kroger, C. Blondel and C. Delsart, *J. Chem. Phys.*, 2005, 122, 014308.
100. R. Otto, A. von Zastrow, T. Best and R. Wester, *Phys. Chem. Chem. Phys.*, 2013, 15, 612-618.
101. J. Wang, J. Li, J. Ma and H. Guo, *J. Chem. Phys.*, 2014, 140, 184314.
102. Z. Lu, J. E. Oakman, Q. Hu and R. E. Continetti, *Mol. Phys.*, 2008, 106, 595-606.
103. M. Van Duzor, F. Mbaiwa, J. Wei, T. Singh, R. Mabbs, A. Sanov, S. J. Cavanagh, S. T. Gibson, B. R. Lewis and J. R. Gascooke, *J. Chem. Phys.*, 2010, 133, 174311.
104. Z. Lu and R. E. Continetti, *Phys. Rev. Lett.*, 2007, 99, 113005.
105. R. Reichle, H. Helm and I. Y. Kiyan, *Phys. Rev. Lett.*, 2001, 87, 243001.
106. S. Miyabe, D. J. Haxton, K. V. Lawler, A. E. Orel, C. W. McCurdy and T. N. Rescigno, *Phys. Rev. A*, 2011, 83, 043401.
107. J. Ma and H. Guo, *Chem. Phys. Lett.*, 2011, 511, 193-195.
108. J. Ma, J. Li and H. Guo, *Phys. Rev. Lett.*, 2012, 109, 063202.
109. C. J. Johnson and R. E. Continetti, *J. Phys. Chem. Lett.*, 2010, 1, 1895-1899.
110. J. P. Maillard, J. Chauville and A. W. Mantz, *J. Mol. Spec.*, 1976, 63, 120-141.
111. H. E. Fleming and K. N. Rao, *J. Mol. Spec.*, 1972, 44, 189-193.
112. S. Zhang, D. M. Medvedev, E. M. Goldfield and S. K. Gray, *J. Chem. Phys.*, 2006, 125, 164312.
113. X. Wang and J. M. Bowman, *J. Phys. Chem. A*, 2014, 118, 684-689.
114. A. F. Wagner, R. Dawes, R. E. Continetti and H. Guo, *J. Chem. Phys.*, 2014, In Press.
115. M. H. W. Gruebele and R. Bigwood, *Int. Rev. Phys. Chem.*, 1998, 17, 91-145.
116. M. J. Frisch, G. W. Trucks, H. B. Schlegel, G. E. Scuseria, M. A. Robb, J. R. Cheeseman, G. Scalmani, V. Barone, B. Mennucci, G. A. Petersson, et al., Gaussian, Inc., Wallingford CT, Revision A.02 edn., 2009.
117. T. Baer and W. L. Hase, *Unimolecular Reaction Dynamics*, Oxford University Press, New York, 1996.
118. R. Otto, A. W. Ray, J. S. Daluz and R. E. Continetti, *EPJ Tech. Instrum.*, 2014, 1, 3.

TOC Figure for “Spectroscopy and Dynamics of the HOCO Radical: Insights into the OH + CO → H + CO2 Reaction”, C.J. Johnson, R. Otto and R.E. Continetti

CP-PER-06-2014-002593

Significance

Photoelectron-photofragment coincidence experiments coupled with quantum chemistry and dynamics calculations have significantly enhanced our understanding of the reactive intermediate HOCO.